# THE RESPONSE OF TURBULENT BOUNDARY LAYERS TO SMALL TURBULENCE LEVELS IN THE EXTERNAL FREE STREAM

H. U. Meier
Deutsche Forschungs- und Versuchsanstalt für Luft- und Raumfahrt E. V.
Aerodynamische Versuchsanstalt Göttingen
Bunsenstrasse 10, 3400 Göttingen, W-Germany

## Abstract

The influence of grid-generated wind tunnel turbulence on the development of a turbulent boundary layer was studied. The free stream turbulence level was varied in the range of 0.05 to 1 per cent and velocity profiles were measured in sidewall boundary layers for different distances from the nozzle exit at approximately zero pressure gradient in the flow direction. For a fixed transition, the shape parameter, skin friction coefficient, and the wake component were estimated from the boundary layer profiles measured at different free stream turbulence levels.

It was found that for external turbulence levels less than 1 per cent the boundary layer shape parameter and wall shear stress vary with the square of the turbulence intensity rather than in a linear way.

## Nomenclature

| | |
|---|---|
| A | van Driest constant, Eq. (7) |
| $c_f$ | skin friction coefficient, $c_f = 2\tau_w/(\rho_\infty U_\infty^2)$ |
| d | diameter of rods |
| D | outer diameter (height) of a Pitot probe |
| G | shape parameter, Eq. (19) |
| $H_{12}$ | shape parameter, Eq. (14) |
| K | constant in the Velocity Defect Law, Eq. (25) |
| M | mesh size of the grid |
| n | exponent for the decay of turbulence, Eq. (23) |
| $p_d$ | dynamic pressure, $p_d = p_t - p_w$ |
| $p_t$ | Pitot pressure |
| $p_w$ | static pressure, measured at the wall |
| $Re_D$ | Reynolds number, based on free stream conditions and the probe diameter D |
| RMS | Root Mean Square |
| Tu | turbulence level $Tu = \left(\overline{u'^2} + \overline{v'^2} + \overline{w'^2}\right)^{1/2} / \left(3U_\infty^2\right)^{1/2}$ |
| $Tu_1$ | turbulence level $Tu_1 = \left(\overline{u'^2}/U_\infty^2\right)^{1/2}$ |
| $Tu_2$ | turbulence level $Tu_2 = \left(\overline{v'^2}/U_\infty^2\right)^{1/2}$ |
| $Tu_3$ | turbulence level $Tu_3 = \left(\overline{w'^2}/U_\infty^2\right)^{1/2}$ |
| $u_\tau$ | shear stress velocity, $u_\tau = (\tau_w/\rho)^{1/2}$ |
| U | mean velocity in x-direction |
| $\left(\overline{u'^2}\right)^{1/2}$ | fluctuating velocity components in x-direction (RMS-value) |
| $\left(\overline{v'^2}\right)^{1/2}$ | fluctuating velocity components in y-direction (RMS-value) |
| $\left(\overline{w'^2}\right)^{1/2}$ | fluctuating velocity components in z-direction (RMS-value) |
| x, y, z | coordinates normal and parallel to the surface |
| $x_G$ | distance from the grid to the leading edge |
| $x_{LE}$ | distance from the leading edge to the measuring station |
| $x_t$ | distance from the virtual origin of turbulence to the measuring station |
| $x_{vo}$ | distance from virtual origin of turbulence to the leading edge |
| $x_p$, $y_p$ | values in the Preston tube analysis, Eqs. (2-4) |
| $y^*$ | dimensionless wall distance, $y^* = yu_\tau/\nu$ |
| $\delta$ | total boundary layer thickness |
| $\delta_1$ | displacement thickness, Eq. (12) |
| $\delta_2$ | momentum thickness, Eq. (13) |
| $\eta$ | dimensionless wall distance, $\eta = y/\delta$ |
| $\kappa$ | von Kármán constant, $\kappa = 0.4$ |
| $\mu$ | dynamic viscosity, $\mu = \nu\rho$ |

| | |
|---|---|
| $\nu$ | kinematic viscosity |
| $\pi$ | wake factor, Eq. (6) |
| $\pi_2$ | constant, Eq. (9) |
| $\rho$ | density |
| $\tau$ | shear stress |
| $\omega$ | wake function, Eq. (6) |
| $\omega_2$ | additional velocity distribution, Eq. (9) |

Subscripts

| | |
|---|---|
| LE | leading edge |
| w | wall conditions |
| $\infty$ | free stream conditions |
| o | conditions at quiescent flow, Tu = 0 |

## 1. Introduction

The influence of external free stream turbulence Tu on a boundary layer is a well known phenomenon. Recent investigations have been concentrated on relatively high turbulence levels of the external stream in order to simulate the flow condition about an airfoil situated in the downstream stages of multistage turbomachinery. A paper by Schlichting and Das[1] deals with the influence of turbulence levels on the aerodynamic losses of axial turbomachines. Systematic investigations of the effect of grid generated turbulence on the development of flat plate boundary layers were carried out by G. Charney et al[2] (Tu = 0.3 % - 5 %) and G. D. Huffman et al[3] (Tu = 1 % - 5 %). However, in connection with the proposal of a large European transonic wind tunnel based on the "Ludwieg Tube" concept P. Bradshaw[4] brought the question into discussion of whether the expected relatively high turbulence level in wind tunnels (Tu < 1 %) will have a strong influence on the experimental results. If significant differences exist between the wind tunnel and atmospheric environments an influence may be mainly exerted upon:

- the change of transition from laminar to turbulent boundary layer flow due to the external turbulence,
- the change of the turbulence structure in the boundary layer with increasing turbulence level which can result for example, in changes of the shape parameter and skin friction coefficient.

While the transition problem with respect to higher external turbulence has not been investigated so far, Charney and Huffman[2, 3] found some systematic changes in the boundary layer development as the turbulence level is varied in the range of Tu ~ 1 % - 5 %. J. E. Green[5] made an analytical study on the basis of these experiments and found - extrapolating the result to quiescent air flows (Tu = 0) - that the local skin friction coefficient $c_f$ at Tu = 0.2 % is roughly 1 % greater than at Tu = 0, while the shape parameter $H_{12}$ is roughly 0.5 % lower. Similar results were obtained in an analytical study by Y. Aihara[6] based on an integral method of solution combined with a perturbation procedure. However, no experimental program has been undertaken to test the validity of either of these analytical results for Tu < 1 %. For this reason a current investigation at the DFVLR-AVA has been concerned with the effect of low free stream turbulence (Tu < 1 %) in subsonic incompressible flow along a flat tunnel wall, upon boundary layer development. The basic turbulence level in the tunnel of Tu ~ 0.04 % was increased by means of various grids having approximately identical mesh sizes. First a careful study of the decay of the turbulence intensity and its deviation from isotropy was made. Then velocity profiles in sidewall boundary layers at different distances from the leading edge and turbulence levels of the external flow were measured. The calculated boundary layer characteristics gave some information about the influence of the external turbulence.

## 2. Description of the Experiments and Data Analysis

### 2.1 Fluid Mechanical Apparatus

The low turbulence wind tunnel of the DFVLR-AVA is of an Eiffel type (Fig. 1). The settling

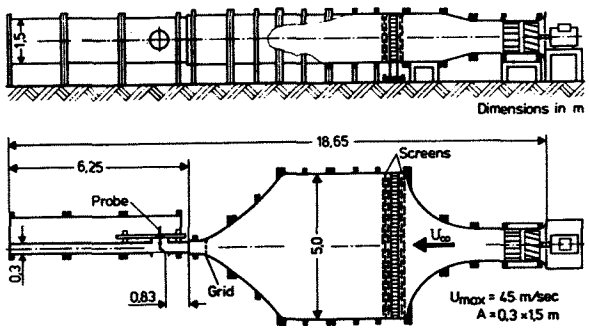


Fig. 1 Low turbulence wind tunnel of the DFVLR-AVA

chamber is equipped with dust filters and screens. The contraction ratio of the test section to the settling chamber is 1:15, in order to obtain a low turbulence level in the free stream. The test section is 0.3 x 1.5 $m^2$. There is a small gap between the nozzle exit and the plane vertical wind tunnel wall (compare Fig. 2). This allows a new wall boundary layer to start at that location. Near the end of the nozzle contraction grids can be installed (Fig. 2) in order to generate turbulence. Due to the remaining contraction (1:1.38) the turbulent motion will undergo selective changes in its axial and transverse turbulent energy levels due to the directionally

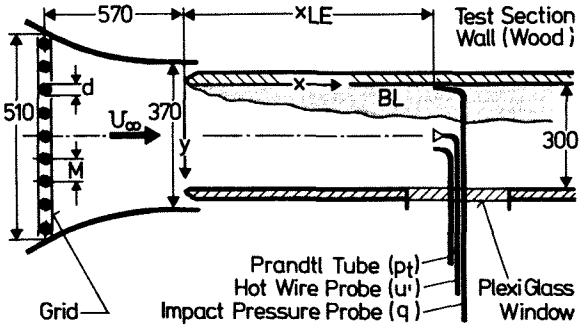

Fig. 2 Sketch of the test section

selective vortex line distortion. As pointed out as early as 1932 by L. Prandtl[7] a contraction in a tube amplifies the transverse-velocity fluctuations relative to longitudinal ones. In this way the grid generated turbulence becomes more isotropic.

The tunnel walls are sufficiently divergent so that only negligible axial pressure and mean velocity gradients exist.

The transition from laminar to turbulent boundary layer flow was fixed 120 mm from and parallel to the leading edge by glueing a plastic tape with embossed large letter V's (tip against flow direction).

## 2. 2 Mean Flow Measurements

The pressure data in the boundary layer were obtained with a flattened Pitot tube having a height of $D = 0.16$ mm. In order to take into account small variations of the free stream, the mean velocity ($U_\infty = 20$ m/s) was measured with a Prandtl tube. The static pressure of the Prandtl tube was taken as the reference pressure for the Pitot tube. Thus in the data reduction procedure the actual free stream velocity could be used for example, to calculate the boundary layer integral values. All data were time averaged over a period of six seconds and then recorded at the identical time with a digital data logging system (AVA), essentially consisting of ten digital voltmeters with a special data storage. This degree of care in the experimental procedure was necessary because only small effects on the boundary layer due to the variation in the low external turbulence level could be expected.

## 2. 3 Turbulence Measurements

Velocity fluctuations in the flow direction (x-direction) were measured with a single hot wire, and in the y- and z-directions with X-hot wires. The hot wire probes were connected to a constant temperature anemometer unit from Thermosystems Inc. (TSI). The output was obtained from a Root Mean Square (RMS)-voltmeter from TSI which enabled measurements of the true RMS-values, $\left(\overline{u'^2}\right)^{1/2}$, $\left(\overline{v'^2}\right)^{1/2}$, $\left(\overline{w'^2}\right)^{1/2}$, to be determined from the fluctuating components u', v', w'. Application of a hot wire for flows with low turbulence levels requires a very careful calibration, as indicated RMS-values at zero velocity ($U_\infty = 0$) are the sum of the instrumentation noise and signals due to the flow around the hot wire caused by natural convection. No way was found to overcome this problem using a proper calibration procedure. Thus the RMS-values for $U_\infty = 0$ were controlled by applying an extrapolation from the calibration curve. From a frequency analysis it was found that a relatively large contribution of the RMS-reading was due to high frequency noise. Due to the fact that these high frequencies ($f > 20$ kHz) cannot result from the flow unsteadiness, a low pass filter with a maximum frequency of 5 kHz was inserted.

The hot wires were recalibrated at each measuring station over the entire velocity range ($U_{\infty\,max} = 45$ m/s with no grid and $U_{\infty\,max} = 36$ m/s with the largest grid). The turbulence levels seemed to show no dependence on the free stream velocity for $U_\infty > 8$ m/s.

The change of the free stream temperature was less than 1 °C during one calibration run. Thus no temperature correction was incorporated into the calibration procedure.

## 2. 4 Determination of the Skin Friction

Because the discussion about the influence of increasing free stream turbulence is often concentraed on the wall shear stress; a special emphasis was placed on this investigation. Two different methods to determine the skin friction have been applied to the measurements reported here.

- Determination from the dynamic pressure measured by a surface Pitot probe (Preston tube).
- Determination from the measured total pressure distributions near the surface.

### 2. 4. 1 Surface Pitot Tubes

In our investigation we were mainly interested in the change of the local skin friction and not necessarily in the absolute values. Thus, due to its simplicity the so called "Preston tube" technique for the evaluation of the wall shear stress was applied. The basis of this method is the universal Law of the Wall, according to which the surface shear stress can be related to the dynamic pressure $p_d$. $p_d$ is the difference between the pressure measured by a Pitot tube resting on the wall ($p_t$) and the wall static pressure ($p_w$).

J. H. Preston's[8] suggestion was that for incompressible turbulent boundary layers on smooth surfaces there exists the universal relation

$$\frac{p_d D^2}{4\rho\nu^2} = \Phi\left(\frac{\tau_w D^2}{4\rho\nu^2}\right) \quad , \qquad (1)$$

where $D$ is the height of the probe and $\tau_w$ is the wall shear stress. Thus $\tau_w$ can be determined once the calibration function $\Phi$ is established. The applicability of the Preston tube technique is discussed by A. Bertelrud[9] in a survey report. He recommends as the best incompressible Preston tube calibration Patel's[10] results. It should be noted that the "calibration function" includes displacement and scale effects of the Pitot tube resting at the surface.

The following notation for the data reduction was used, following Eq. (1)

$$x_p = \log \frac{p_d D^2}{4\rho\nu^2} \quad . \qquad (2)$$

Using Patel's calibration curve

$$x_p = y_p + 2 \log (1.95\, y_p + 4.1) \quad , \qquad (3)$$

valid for the range $3.5 < y_p < 5.3$. $\tau_w$ can be calculated implicitily from the relation

$$y_p = \log \frac{\tau_w D^2}{4\rho\nu^2} \quad . \qquad (4)$$

Then we obtain the local skin friction coefficient as

$$c_f = \frac{\tau_w}{(\rho_\infty/2)U_\infty^2} = \frac{8 \cdot 10^{y_p}}{Re_D^2} \quad , \qquad (5)$$

where $Re_D$ is the free stream Reynolds number based on the probe height ($Re_D = U_\infty D/\nu$).

The Preston tube technique offers the advantage that the skin friction can be determined from a single measurement. However, the Preston tube readings can be effected by

- displacement effects of the probe,
- tube size, $D$,
- ratio of the inner to outer probe diameter,
- pressure gradients, $dp/dx$,
- three-dimensional flow effects.

Due to the fact that in our experiment the probe effects were approximately identical since only the turbulence of the external flow was changed, the conditions listed above will have no effect on the qualitative validity of the experimental results. However, the results were proved using a more advanced technique described in the following section.

### 2. 4. 2 Determination of Local Skin Friction from Experimental Velocity Profiles

The basis of the scheme is the comparison of calculated velocity profiles which are constructed from the Law of the Wall and Coles's Law of the Wake[11] with measured profiles. An additional distribution, $\omega_2(y/\delta)$, was introduced for the description of the wake by J. C. Rotta in order to elimate the abrupt change in the slope $\partial u/\partial y$ at the outer edge of the boundary layer. The entire profile then may be constructed following the relation

$$\frac{U}{u_\tau} = f(y^*) + \frac{\pi}{\varkappa}\omega(\eta) + \frac{\pi_2}{\varkappa}\omega_2(\eta) \quad . \qquad (6)$$

Here the function $f$ represents the Law of the Wall and is a function of the dimensionless distance, $y^* = yu_\tau/\nu$. ($y$ is the wall distance, $u_\tau = \sqrt{\tau_w/\rho}$ shear stress velocity, and $\nu$ the kinematic velocity.) If the viscous sublayer is included by introducing a van Driest's damping function to the mixing length, the Reynolds shear stress can be approximated by

$$-\overline{u'v'} = (\varkappa y)^2 \left[1 - \exp\left\{-y\frac{u_\tau}{\nu A}\right\}\right]^2 \left|\frac{dU}{dy}\right| \frac{dU}{dy} \quad . \qquad (7)$$

Then we can calculate the function $f$ from the relation

$$\frac{df}{dy^*} = \frac{\nu}{u_\tau^2}\frac{dU}{dy} = \frac{2}{1 + \sqrt{1 + 4\varkappa^2\left\{y^*\left[1 - \exp\left(-\frac{y^*}{A}\right)\right]\right\}^2}} \qquad (8)$$

where $\varkappa$ is the von Kármán and $A$ the van Driest constant, respectively.

In the Coles wake function $\omega(\eta)$, $\eta$ is the dimensionless wall distance $y/\delta$. At the leading edge $\omega(\eta = 1)$ becomes 2 while $\omega(\eta = 0)$ at the surface is 0. The distribution $\omega_2(\eta)$ is given by

$$\omega_2(\eta) = (\eta)^5(1 - \eta)(4\eta - 3) \quad . \qquad (9)$$

The constant, $\pi_2$, can be derived from the boundary condition

$$y = \delta \rightarrow \frac{dU}{dy} = u_\tau\left[\frac{df}{dy^*}\frac{u_\tau}{\nu} - \frac{\pi_2}{\varkappa}\frac{1}{\delta}\right] = 0 \quad . \qquad (10)$$

The local skin friction law is obtained from Eq. (6) for $\eta = 1$

$$\sqrt{\frac{2}{c_f}} = \frac{U_\infty}{u_\tau} = f\left(\frac{\delta u_\tau}{\nu}\right) + 2\,\frac{\pi}{\varkappa} \quad . \tag{11}$$

If the values $U_\infty$, $\nu$, $\varkappa$, A are given we can determine any one of the three parameters $u_\tau$, $\delta$, and $\pi$, if the other two are known. This leads to the consideration of using Eqs. (6) and (11) in conjunction with experiments as was proposed by J. C. Rotta[12]. If the velocity profiles are constructed using Eq. (6) the wall shear stress and the boundary layer thickness have to be determined in such a way that the calculated profile is in the best possible agreement with the experimental one. This is accomplished by requiring that the Root Mean Square deviation between the two profiles becomes a minimum. In addition an iterative procedure can be applied in order to solve the nonlinear problem of finding the most probable values of $u_\tau$, $\delta$, $\pi$, A, and $\varkappa$. This enables one to make a statistical analysis of the experimental velocity profile. In our case the values of $\varkappa$ and A were assumed to be constant ($\varkappa = 0.4$, $A = 26.5$), because there is no reason to believe that they will change with increasing free stream turbulence.

Once the shear stress and the boundary layer has been obtained by such a procedure, all other boundary parameters such as the displacement thickness

$$\delta_1 = \int_{y=o}^{y=\delta} \left(1 - \frac{U}{U_\infty}\right) dy \tag{12}$$

and the momentum thickness

$$\delta_2 = \int_{y=o}^{y=\delta} \frac{U}{U_\infty}\left(1 - \frac{U}{U_\infty}\right) dy \tag{13}$$

can be calculated. Then the shape parameter defined as

$$H_{12} = \frac{\delta_1}{\delta_2} \tag{14}$$

can be calculated from Eqs. (12) and (13).

## 3. Prediction Methods

Most of the available calculation methods for the prediction of the effect of the free stream turbulence shear layers have already been discussed in a review paper by P. Bradshaw[13]. His study led to the conclusion that the existing information about mean-flow properties and turbulence had not been fully absorbed into the calculation methods. Two papers which were recently published should be added to the list of references in Ref. 13. First D. Arnal et al[14] investigated boundary layer development with positive pressure gradient in a turbulent external flow. They compared their experimental results by means of a set of transport equations and an integral method in which an adapted mixing length scheme is used. The other analytical study of a turbulent boundary layer along a flat plate with external flow turbulence was carried out by Y. Aihara[6]. He used an integral method of solution with first and second order perturbation procedures for his investigation of the effect of small external flow turbulence. In Ref. 6 results are presented based on a simple formula for the mixing length ($l/\delta = \varkappa y/\delta$). In the mean time Y. Aihara derived - by means of the same procedure - relations which include a modification of the mixing length formula ($l/\delta = 0.09 \tanh(\varkappa\zeta/0.09)$). The calculations lead to the following results:

$$\frac{\delta_1 - (\delta_1)_{Tu=o}}{(\delta_1)_{Tu=o}} = 7.58\ Tu \quad , \tag{15}$$

$$\frac{\delta_2 - (\delta_2)_{Tu=o}}{(\delta_2)_{Tu=o}} = 10.0\ Tu \quad , \tag{16}$$

$$\frac{\Delta H_{12}}{(H_{12})_o} = \frac{H_{12} - H_{12,\,Tu=o}}{H_{12,\,Tu=o}} = -2.43\ Tu \quad , \tag{17}$$

and

$$\frac{\Delta c_f}{cf_o} = \frac{c_f - (c_f)_{Tu=o}}{(c_f)_{Tu=o}} = 3.84\ Tu \quad . \tag{18}$$

A second claculation method has been proposed by J. E. Green[5]. His analysis of the measurements of Huffman et al shows that the shape parameter

$$G = \frac{H_{12} - 1}{H_{12}}\sqrt{\frac{2}{c_f}} \quad , \tag{19}$$

varies as

$$G = G_o\left(1 + \frac{1}{3}\sqrt{\frac{2}{c_f}}\,\frac{\sqrt{\overline{u'^2}}}{U_\infty}\right) \quad . \tag{20}$$

Taking $G_o$ as 6.4 in quiescent air he found that the influence of increasing free stream turbulence on the local skin friction can be described as

$$\frac{\Delta c_f}{c_{fo}} = 4.8\ Tu \quad . \tag{21}$$

If Eq. (21) is applied for low external turbulence ($Tu \to 0\ \%$) it must be noted that the corresponding shape factor G is obtained from a linear extrapolation based on Huffman's experiments performed at turbulence levels in the range of $1\ \% < Tu < 5\ \%$.

## 4. Results

### 4.1 Turbulence Measurements

The turbulence level in the wind tunnel was investigated with and without grids. Four different grid sizes were used. The geometry was varied in such a way that the difference (M - d) between mesh-size M and the wire diameter d was approximately constant. In Fig. 3 the measured turbu-

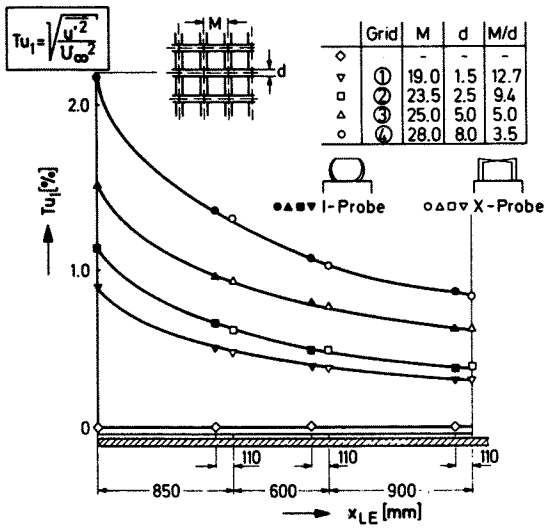


Fig. 3 Decay of the turbulence level $Tu_1 = \sqrt{u'^2/U_\infty^2}$ downstream of grids

lence levels in the wind tunnel with and without grids for different distances from the leading edge are shown. The pressure gradient in flow direction at $U_\infty \approx 20$ m/s was approximately zero. The black symbols indicate measurements with a single hot wire probe while the open symbols represent results from an X-hot wire probe. The results of the single wire probe and those of the X-wire probe are in the range of the expected accuracy.

An anisotropic external turbulence could result in a different mass entrainment process than an isotropic one. Therefore the existence of quasi isotropic turbulence in the investigated tunnel flow was to be established. The v' and w' fluctuating velocity components were measured with X-hot-wires. The results of these turbulence measurements are shown in Fig. 4 and 5. The decay of the fluctuating velocity components v' and w' in y- and z-direction with increasing distance from the leading edge is similar to that of the u'-velocity component. However, as shown in Fig. 6, the measurements indicated that the ratio of the longitudinal to lateral turbulent intensities is consistently larger than 1.0 for distances $x_{LE} \leq 1\,500$ mm. This result is qualitatively in agreement with published results of anisotropic grid turbulence. Uberoi[15] found by measurements of turbulence behind a square-mesh biplane grid made of round rods that the RMS turbulent velocity fluctuations are characterized by

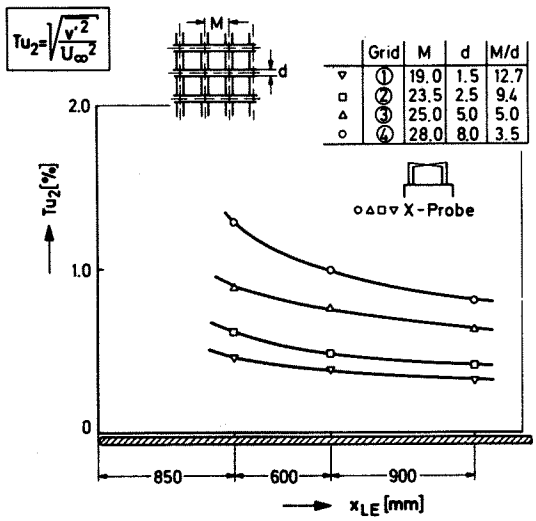


Fig. 4 Decay of the turbulence level $Tu_2 = \sqrt{v'^2/U_\infty^2}$ downstream of grids

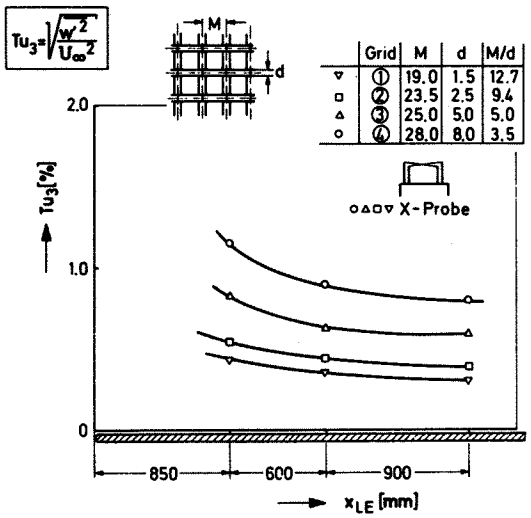


Fig. 5 Decay of the turbulence level $Tu_3 = \sqrt{w'^2/U_\infty^2}$ donwstream of grids

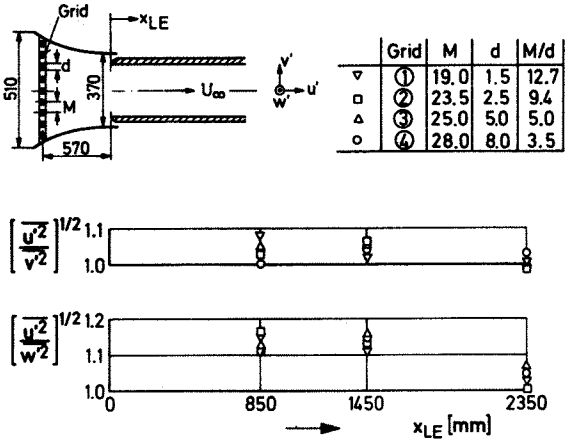


Fig. 6 Decay of anisotropy for the grid generated turbulence

$$\left(\overline{v'^2}\right)^{1/2} = \left(\overline{w'^2}\right)^{1/2} = \frac{\left(\overline{u'^2}\right)^{1/2}}{1.18} \quad . \qquad (22)$$

However, in our experiment the $\left(\overline{v'^2}\right)^{1/2}$-component is greater than the $\left(\overline{w'^2}\right)^{1/2}$-component. This result can be explained by the special geometry of the wind tunnel test section whose dimension in the z-direction is about five times of that in the y-direction. (The measurements of Uberoi were made in an axisymmetric nozzle.) As indicated in Fig. 6 the tunnel turbulence has become quasi isotropic*) by a distance of $x_{LE} \sim 2\,000$ mm only for the small grids ① and ②. The turbulence generated by the largest investigated grids ③ and ④ yields a fluctuating velocity component, w', which is smaller even at this distance. This result is not in agreement with experiments carried out by Portfors and Keffer[16] who found already isotropic turbulence at a distance from the leading edge of about 30 mesh lengths [30 M ≙ ($x_{LE} \sim 600$ mm)]. Clearly, the experimental verification of isotropy depends upon the accuracy to which the three components of turbulent intensity can be determined. In Ref. 16 it is demonstrated that the experimental results depend strongly on the applied measuring technique and data reduction procedure. However, the authors of Ref. 16 found that for distances $x_G/M \leq 20$ (where $x_G$ is the distance from the grid to the measuring station) the ratios of the longitudinal to lateral components $\left(\overline{u'^2}\right)^{1/2}/\left(\overline{w'^2}\right)^{1/2}$ are greater than unity, while the RMS-values of $\left(\overline{u'^2}\right)^{1/2}/\left(\overline{v'^2}\right)^{1/2}$ are considerably smaller than unity. This was found neither by Uberoi[15] nor in the here described experiments.

If simple theoretical relations for the decay of the turbulence intensity $Tu_1 = \sqrt{\overline{u'^2}}/U_\infty$ are to be applied, the distance from the virtual origin, at which $Tu_1 = \infty$, to the grid has to be known.

In order to find this virtual origin it was assumed - following Rotta[17] - that the decay of the RMS-values of the measured longitudinal velocity fluctuations $\left(\overline{u'^2}\right)$ is proportional to $(x_{LE})^{-n}$. Comte-Bellot and Corrsin[18] found values for n in the range of $n = 1.2$ and $n = 1.3$. In Fig. 7 the calculated values of $\left(\overline{u'^2}\right)^{-(1/n)}$, where $n = 1.3$, for the four different investigated grids are plotted versus the distance from the leading edge $x_{LE}$. The points were approximated by

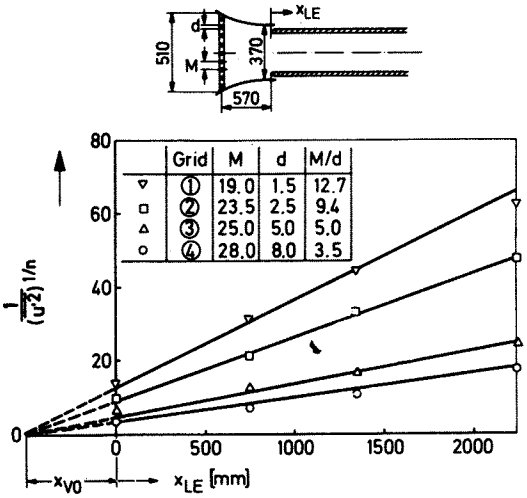


Fig. 7 Evaluation of the virtual origin $x_{vo}$ of turbulence for different grids ($n = 1.3$)

straight lines and the distance $x_{vo}$ from the grid to the virtual origin was found to be approximately 500 mm. The slope of the straight lines in Fig. 7 indicated that the measured turbulence data for the different grids could be correlated by multiplying the distance ($x_t = x_{LE} + x_{vo}$) by the grid-parameter M/d. The result is shown in Fig. 8. The

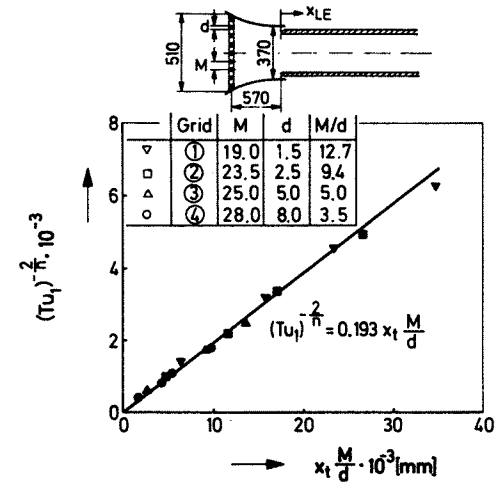


Fig. 8 Decay of the turbulence level $Tu_1$ downstream of different grids ($n = 1.3$)

decay of turbulence intensity of all three grids can be correlated and described by the relation

$$\left(Tu_1\right)^{-2/n} = 0.193\left[(x_{LE} + x_{vo})\frac{M}{d}\right] \quad . \qquad (23)$$

## 4.2 Boundary Layer Mean Flow Measurements

Boundary layer velocity profiles were measured along the center line of the tunnel sidewall (compare Fig. 1). The measurements were made at constant pressure along the plate and a free stream

*) Actually, true isotropy requires more than equality of the intensity components alone. Their energy spectra must be related through the isotropic expressions over the complete wavenumber range of turbulence. This analysis was, however, not carried out.

velocity of $U_\infty$ = 20 m/s , for three different distances from the leading edge. The experimental data were reduced and analyzed so that the effects of the external turbulence level on the boundary layer development could be studied and compared with theoretical results. The "integral" properties were calculated using the approximated theoretical profiles obtained from the procedure described in Section 2. 4. 2. The advantage of this procedure is that the extrapolation from the last measured point towards the wall is physically meaningful and not arbitrary. The integral properties obtained from measured boundary layer profiles at three different distances from the leading edge, using four different grids for each station are compiled in Table 1. First of all the change of the profile due to increasing free stream turbulence shall be considered.

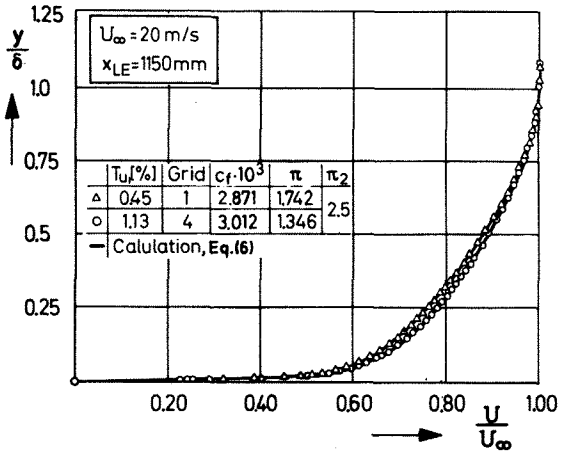


Fig. 9 The influence of external turbulence on the mean velocity profile development

In Fig. 9 two velocity profiles are shown which were measured at a distance of 1.150 m from the leading edge at free stream turbulence levels $Tu_1$ = 0. 45 % and $Tu_1$ = 1. 13 % . With increasing external turbulence the profile becomes fuller. The measured profiles are compared with calculated ones in accordance with Eq. (6). The empirical constants $\pi$ and $\pi_2$ as well as the boundary layer thickness and the skin friction coefficient are obtained by the statistical analysis described in Sect. 2. 4. 2. For all calculations the von Kármán constant was assumed to be invariant ($\varkappa$ = 0. 4) . From Table 1 the corresponding integral thickness $\delta_1$, $\delta_2$ show an overall slight decrease with increasing external turbulence. However, no unique tendency is apparent if the integral thickness at intermediate turbulence levels are considered. The actual reason for this is the fact that the change of the velocity profile due to change in $Tu_1$ is small. This is demonstrated by plotting for the same two profiles the local momentum loss versus the distance y (Fig. 10). It can be seen from this figure that the smaller local momentum loss of the fuller velocity profile at Tu = 1. 13 % is partly compensated by the increase of the boundary layer thickness. The application of various techniques for the estimation of the boundary layer thickness can result in errors of the calculated integral thicknesses which are of order of expected effects due to the change in the turbulence level. However, it is clear from Table 1 that the shape parameter

Table 1 Results of boundary layer profile measurements ($U_\infty$ = 20 m/s)

| $x_{LE}$ [mm] | Grid | $Tu_1$ [%] | δ [mm] | $\delta_1$ [mm] | $\delta_2$ [mm] | $H_{12}$ [-] | $c_f \cdot 10^3$ [-] | π [-] |
|---|---|---|---|---|---|---|---|---|
| 850 | - | 0. 04 | 18. 75 | 2. 923 | 2. 053 | 1. 424 | 3. 037 | 1. 598 |
| | ① | 0. 51 | 18. 51 | 2. 904 | 2. 035 | 1. 427 | 3. 034 | 1. 626 |
| | ② | 0. 63 | 18. 78 | 2. 912 | 2. 049 | 1. 422 | 3. 047 | 1. 566 |
| | ③ | 0. 92 | 19. 99 | 3. 000 | 2. 133 | 1. 406 | 3. 081 | 1. 403 |
| | ④ | 1. 29 | 18. 93 | 2. 840 | 2. 018 | 1. 400 | 3. 131 | 1. 307 |
| 1150 | - | 0. 04 | 22. 53 | 3. 514 | 2. 477 | 1. 419 | 2. 890 | 1. 722 |
| | ① | 0. 45 | 23. 38 | 3. 634 | 2. 571 | 1. 417 | 2. 871 | 1. 716 |
| | ② | 0. 55 | 24. 59 | 3. 784 | 2. 683 | 1. 411 | 2. 858 | 1. 691 |
| | ③ | 0. 83 | 24. 73 | 3. 704 | 2. 648 | 1. 399 | 2. 921 | 1. 524 |
| | ④ | 1. 13 | 23. 99 | 3. 501 | 2. 519 | 1. 390 | 3. 012 | 1. 346 |
| 1450 | - | 0. 04 | 27. 20 | 4. 088 | 2. 925 | 1. 398 | 2. 842 | 1. 203 |
| | ① | 0. 40 | 26. 21 | 3. 978 | 2. 835 | 1. 403 | 2. 854 | 1. 635 |
| | ② | 0. 49 | 27. 57 | 4. 278 | 3. 055 | 1. 400 | 2. 860 | 1. 516 |
| | ③ | 0. 76 | 28. 92 | 4. 233 | 3. 053 | 1. 386 | 2. 868 | 1. 470 |
| | ④ | 1. 02 | 28. 11 | 4. 075 | 2. 946 | 1. 383 | 2. 912 | 1. 383 |

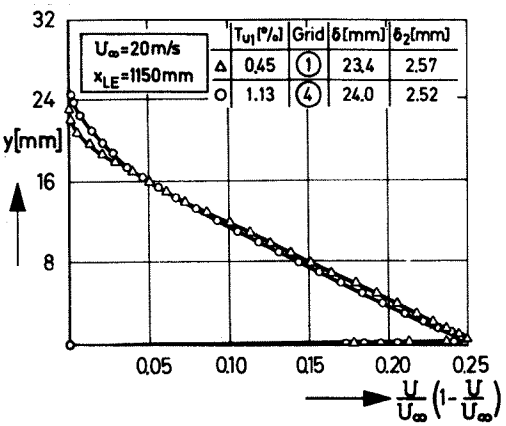


Fig. 10 The local momentum loss in a boundary layer at two different free stream turbulence levels

$H_{12}$ shows a unique tendency, it is steadily decreasing with increasing free stream turbulence.

The Law of the Wall representation, $U/u_\tau$ versus the dimensionless wall distance $y^*=yu_\tau/\nu$, clearly indicates an influence of $Tu_1$ on the so-called wake region of the boundary layers. In Fig. 11 again the two measured profiles are compared with each other and with calculated ones. The wake component $\pi$ decreases for the two profiles with increasing Tu, from $\pi = 1.74$ to $\pi = 1.35$, and would go to zero for even larger values of Tu. This effect of Tu on the boundary layer profile appears more clearly in the defect law representation, Fig. 12. The velocity defect $(U_\infty - U)/u_\tau$ is plotted versus $yu_\tau/(\delta_1 U_\infty)$. The values for $c_f$ and $\delta_1$ were obtained from the calculated profiles shown in Fig. 11. It can be seen from Fig. 12 that the universal Law of the Wall and its concept of a single-parameter velocity profile can be applied to the velocity defect defined as follows:

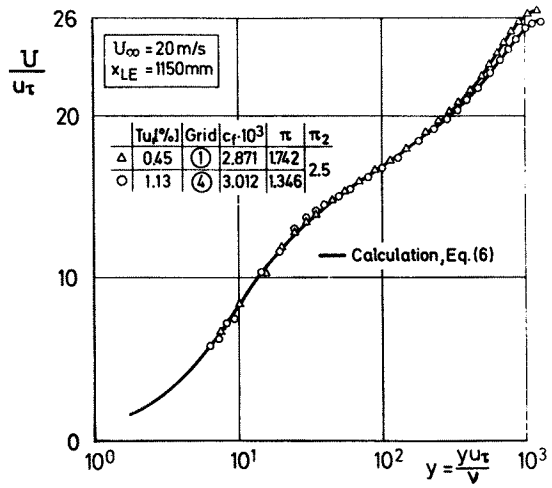


Fig. 11 Logarithm representation of mean velocity profiles for two different free stream turbulence levels

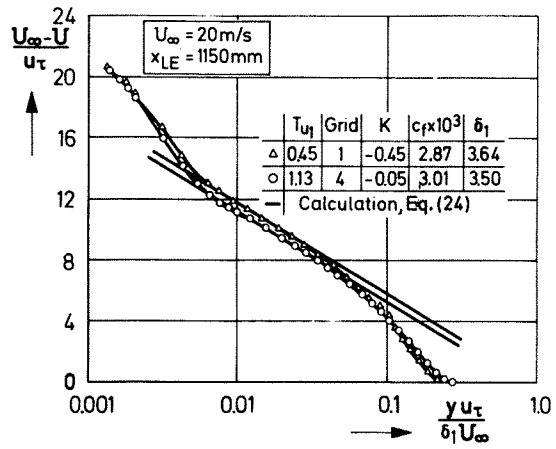


Fig. 12 Measured velocity defect profiles of a turbulent boundary layer at different turbulence levels compared with calculations based on Eq. (25)

$$\frac{U_\infty - U}{u_\tau} = \Phi\left(\frac{yu_\tau}{\delta_1 U_\infty}\right) \quad . \tag{24}$$

The constant K in

$$\frac{U_\infty - U}{u_\tau} = -\frac{1}{\kappa}\ln\frac{yu_\tau}{\delta_1 U_\infty} + K\left(\frac{u_\tau}{U_\infty}\right) \tag{25}$$

was derived from the drawing. It becomes almost zero for the turbulence level $Tu_1 = 1.13\,\%$. In order to get some general information about the results given in Table 1 the analysis of J. E. Green[5] was applied. Essentially he calculated the shape parameter G (Eg. (19)), from Huffman's et al experimental results given in Ref. 3. The variation of G with $\sqrt{u'^2}/u_\tau$ was compared with a linear function following Eq. (20), (see Fig. 13). At first

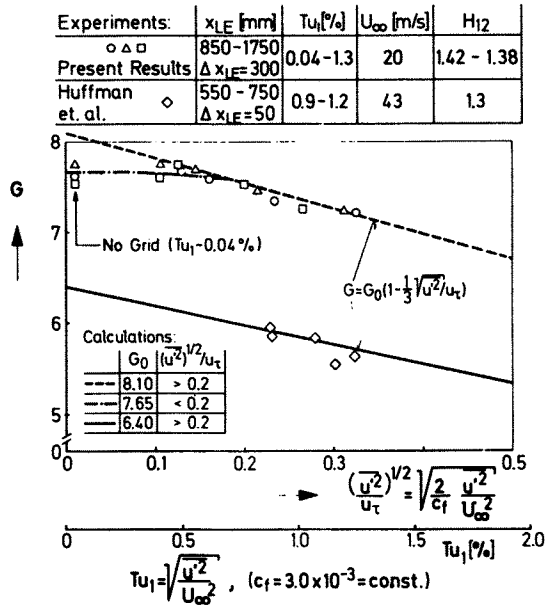


Fig. 13 The influence of changes in the free stream turbulence on the shape parameter G

glance there is a considerable difference between Green's results and ours. But the main deviation is due only to the different profile families which were investigated. While Huffman's[3] et al and Carnay's[5] et al experiments were performed in wind tunnels with approximately square test sections, the tunnel we used had a rectangular test section. The shape parameters of Refs. 3 and 5 are in the order of $H_{12} \sim 1.3$ while we got values of $H_{12} \sim 1.4$. No explanation can be offered for the relatively high values of $G_o$. However, the measurements of Ludwieg and Tillmann[19] and of Wieghardt (collected in Coles[20] Stanford Conference Data Compilation) were performed in a similar rectangular tunnel, and show almost identical values of the shape parameter $H_{12}$.

The main information we can obtain Fig. 13 is that the suggestion of a linear increase of $G$ with decreasing turbulence level $Tu < 1\,\%$ is not confirmed by the experimental results. Bradshaw's argument namely that uncorrelated disturbances contribute as mean squares rather than as RMS-values and that therefore at turbulence intensities in normal subsonic wind tunnels ($Tu_1 < 1\,\%$) the effect should vary as $\overline{u'^2}$ rather than as $(\overline{u'^2})^{1/2}$ is supported through these results. The fact is that values of $G$ obtained at very low turbulence levels ($Tu_1 \sim 0.04\,\%$) are sometimes even smaller compared to G-values obtained from profile measurements using the smallest grid. This leads to the supposition that the turbulence structure of the boundary profile is changed due to external artificial turbulence. It is indicated in Fig. 13 that the G-values for $Tu_1 > 1.0\,\%$ can be approximated using the same linear curve fit proposed by Green, while for the range $0 < (\overline{u'^2})^{1/2}/u_\tau < 0.2$ a quadratic law should be used. However, if the percentage deviation of the shape parameter $(G - G_o)/G_o$ instead of $G$ is plotted versus $(\overline{u'^2})^{1/2}/u_\tau$, Huffman's and our measurements will match with each other, as demonstrated in Fig. 14. The shape parameter $G_o$ at quiescent air flow has to be evaluated using an extrapolation to $Tu_1 = 0$ of G-values computed from measured profiles. In our case $G_o$ was taken to be 8.1 (compare Fig. 13). The experimental data for $Tu_1 < 1\,\%$, $(\overline{u'^2})^{1/2}/u_\tau \approx 0.26$, were approximated using a curve fit following the relation

$$\frac{G - G_o}{G_o} = -0.72\left[\frac{(\overline{u'^2})^{1/2}}{u_\tau}\right]^2 - 0.047 \quad , \quad (26)$$

while a linear curve fit of the data for $Tu > 1\,\%$ led to nearly the same result as proposed by J. E. Green.

The skin friction coefficients obtained from the profile analysis show of course almost the same

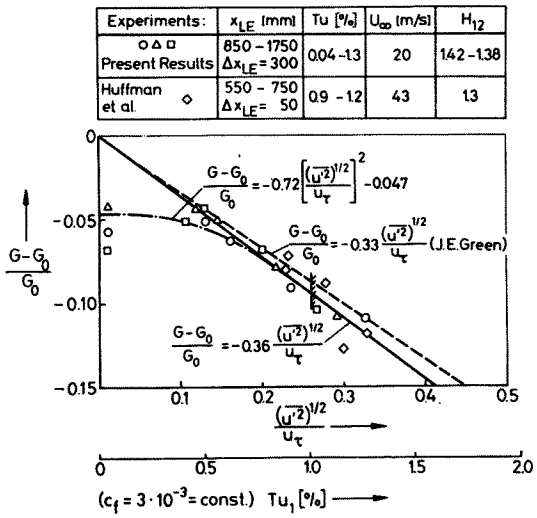


Fig. 14 Percentage deviation of the shape parameter with decreasing turbulence level

trend as the G-values. Thus it seemed to be useful to prove these results applying a direct measuring technique. Despite the limitation of the Preston tube technique, this method did allow us to obtain fast qualitative results*). In Fig. 15 it is indicated

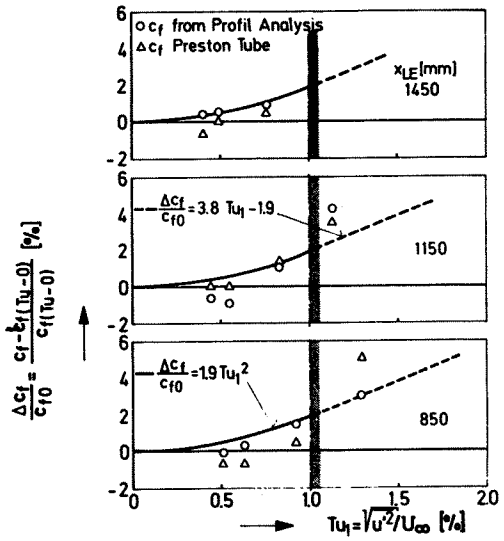


Fig. 15 Comparison of skin friction values obtained from profile and Preston tube measurements

that skin friction coefficients measured with a Preston tube give the same qualitative results as obtained from the profile analysis**). The change in the skin friction coefficients with increasing $Tu_1$ can be described in the following forms:

*) These measurements were performed by R. Fleeter, a student at Brown University, during a two month leave at the DFVLR-AVA, Göttingen.

**) For the data presentation in Fig. 15, $Tu_1 = 0.04$ was taken as $Tu_1 = 0$.

$$\frac{\Delta c_f}{cf_o} = \frac{c_f - (c_f)_{Tu=o}}{(c_f)_{Tu=o}} = 1.9\ Tu_1^2 \quad , \text{ for } Tu_1 < 1\ \% \ , \tag{27}$$

and

$$\frac{\Delta c_f}{cf_o} = 3.8\ Tu_1 - 1.9 \quad , \text{ for } Tu_1 > 1\ \% \ . \tag{28}$$

This is confirmed by comparisons of other prediction methods with the experimental results as demonstrated in Fig. 16. Obviously both prediction

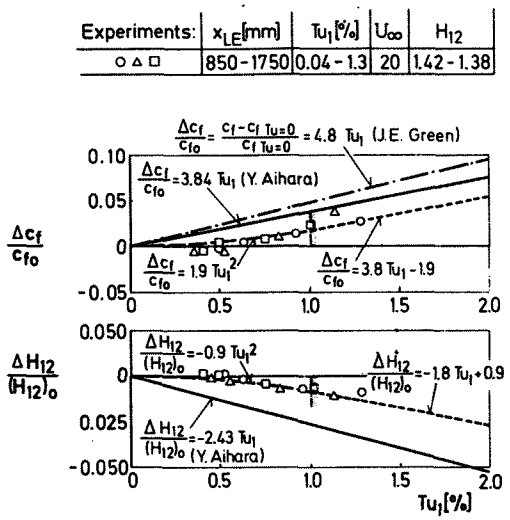


Fig. 16 Comparison between the measured and calculated influences of increasing turbulence levels on the skin friction and shape parameter

methods described in Chap. 3 overestimate considerably the influence of $Tu_1$ on $c_f$ for values $Tu_1 < 1\ \%$. For $Tu_1 > 1\ \%$ our projected slope is in close agreement with that of Y. Aihara[6]. In Fig. 15 the expected decrease of the shape parameter $H_{12}$ with increasing Tu is confirmed, as well. However, again an overestimate upon applying the prediction method of Y. Aihara can be observed. These experimental results were also approximated by curve fits following the relations

$$\frac{\Delta H_{12}}{(H_{12})_o} \quad \frac{H_{12} - (H_{12})_{Tu=o}}{(H_{12})_{Tu=o}} = -0.9\ Tu_1^2 \ , \text{ for } Tu_1 < 1\ \% \tag{29}$$

$$\frac{\Delta H_{12}}{(H_{12})_o} = -1.8\ Tu_1 \times 0.9 \ , \text{ for } Tu_1 > 1\ \% \tag{30}$$

which describe the physical behaviour of the boundary layer development at low turbulence levels in a more sophisticated manner.

## 5. Summary of the Results and Conclusions

The results of the experiments can be summarized as follows:

- The grid generated turbulence in the rectangular wind tunnel was even beyond distances of 200 mesh sizes still only quasi isotropic.
- The boundary layer velocity profiles measured at three different distances from the leading edge and different turbulence levels $Tu_1$ ($0.04\ \% < Tu_1 < 1\ \%$) were successfully approximated by claculated profiles based on the Law of Wall and the Law of the Wake.
- The calculated integral thicknesses $\delta_1$, $\delta_2$ did not show a unique trend with respect to changes in the turbulence level $Tu_1$. However, the shape parameter $H_{12} = \delta_1/\delta_2$ decreases as $Tu_1$ increases.
- The most significant result seems to be that the influence of the external turbulence on gross boundary layer properties decreases considerably for $Tu < 1\ \%$. Thus it is proposed to apply relations in this region in the form $1 + O(\overline{u_1'^2})$ while in the region $Tu_1 > 1\ \%$ a linear relation in the form $1 + O(\overline{u'^2})^{1/2}$ may still be used.
- The percentage deviation of the skin friction coefficient $c_f$ and the shape parameter $H_{12}$ at $0 < Tu_1 < 1\ \%$ compared with values obtained at quiescent flow conditions are listed for convenience in the following table:

| Tu [%] | Eq. (27) $\Delta c_f/c_{fo}$ [%] | Eq. (29) $\Delta H_{12}/(H_{12})_o$ |
|---|---|---|
| 0.2 | 0.08 | - 0.04 |
| 0.5 | 0.48 | - 0.23 |
| 1.0 | 1.90 | - 0.90 |

The experimental investigation has led us to following conclusions:

- Turbulence levels in low speed wind tunnels of less then 0.2 per cent have no measurable influence on the skin friction coefficient and the shape parameter. This result qualitatively is in agreement with results of Schubauer and Skramstad[21] about the influence on the critical Reynolds number on a flate at zero incidence.
- According to the experiments, uncertainties exist as to whether the basic structure of the boundary layer is altered even by the installation of very small grids. A study of the length scale distribution as well as a frequency analysis of the boundary layer should clarify this problem.

- No information was obtained concerning the influence of low external turbulence on the transition from laminar to turbulent boundary layer flow, nor has the additional influence of pressure gradients in flow direction been explored.

- It is clear that although we are dealing with two-dimensional boundary layers, the turbulence is a three-dimensional phenomenon. For this reason, further research should encompass problems encountered in three-dimensional external flow effects.

## References


[1] Schlichting, H. Das, A., On the Influence of Turbulence Level on the Aerodynamic Losses of Axial Turbomachines Flow Research on Blading, Elsevier Publishing Company, Amsterdam-London-New York, 1970, pp. 234-274.

[2] Charnay, G., Comte-Bellot, G., Mathieu, J., Development of a Turbulent Boundary Layer on a Flat Plate in an External Turbulent Flow, AGARD Conf. Proc. 93, Paper No. 27, 1971.

[3] Huffman, G. D., Zimmerman, D. R., Benett, W. A., The Effect of Free Stream Turbulence Level on Turbulent Boundary Layer Behaviour, AGARDograph 164, 1972.

[4] Bradshaw, P., A Note on the Working-Section Turbulence in a Ludwieg Tube, I. C. Aero. Report 74-01, 1974.

[5] Green, J. E., On the Influence of Free Stream Turbulence on a Turbulent Boundary Layer, as it Relates to Wind Tunnel Testing at Subsonic speeds, AGARD Report 602, 1973, pp. 4-1 to 4-8.

[6] Aihara, Y., Analytical Study of a Turbulent Boundary Layer Along a Flat Plate with External Flow Turbulence, DFVLR-AVA Internal Report IB 75 A 33, 1975.

[7] Prandtl, L., Herstellung einwandfreier Luftströme (Windkanäle), Handbuch der Experimentalphysik, Vol. 4, Part 2, Leipzig, 1932.

[8] Preston, J. H., The Determination of Turbulent Skin Friction by Means of Pitot Tubes, J. Roy. Aero. Soc., Vol. 58, 1954, pp. 109-121.

[9] Bertelrud, A., Pipe Flow Calibration of Preston Tubes of Different Diameters and Relative Length Including Recommodations on Data Presentation for Best Accuracy, FFA Report 125, 1974.

[10] Patel, V. C., Calibration of the Preston Tube and Limitations on its Use in Pressure Gradients, J. Fluid Mech., Vol. 23, Part 1, 1965, pp. 185-208.

[11] Coles, D., The Law of the Wake in the Turbulent Boundary Layer, J. Fluid Mech., Vol. 1, 1956, pp. 191-226.

[12] Rotta, J. C., Control of Turbulent Boundary Layers by Uniform Injection and Suction of Fluid, Paper presented at the VIIth Congress of Aeronautical Science (ICAS VII), Rome, 1970.

[13] Bradshaw, P., Effect of Free-Stream Turbulence on Turbulent Shear Layers, Aeronautical Research Council A. R. C. 35 648, 1974.

[14] Arnal, D., Cousteix, J., Michel, R., Couche limite se développant avec gradient de pression positif dans un écoulement extérieur turbulent, La Recherche Aérospatiale, No. 1, 1976, pp. 13-26.

[15] Uberoi, M. S., Small Axisymmetric Contraction of Grid Turbulence, J. Fluid Mech., Vol. 24, part 3, 1966, pp. 539-543.

[16] Portfors, E. A., Keffer, J. F., Isotropy in Initial Period Grid Turbulence, Phys. Fluids, Vol. 12, 1969, pp. 1519-1521.

[17] Rotta, J. C., Turbulente Strömungen, B. G. Teubner Verlag, Stuttgart, 1971.

[18] Comte-Bellot, G, Corrsin, S., The Use of Contraction to Improve the Isotropy of Grid-Generated Turbulence, J. Fluid Mech., Vol. 25, 1966, pp. 657-682.

[19] Ludwieg, H., Tillmann, W., Untersuchungen über die Wandschubspannung in turbulenten Reibungsschichten, Ing. -Arch. 17, 1949, pp. 288-299. Also available as NACA TM 1285, 1950.

[20] Coles, E. D., Hirst, E. A., Computation of Turbulent Boundary - 1968, AFOSR-IFP-Stanford Conference, Stanford University, California, USA, 1969.

[21] Schubauer, G. B., Skramstad, H. K., Laminar Boundary Layer Oscillations and Stability of Laminar Flow, J. Aero. Sci., Vol. 14, 1947, pp. 69-78; see also NACA Rep. No. 909, 1948.


## Acknowledgement


The author would like to express his appreciation to Dr. J. C. Rotta for many beneficial discussions and wants to thank Mr. D. Baumgarten, who was responsible for the accomplishment of the measurements and data reduction.